



GLOBAL JOURNAL OF RESEARCHES IN ENGINEERING: A
ELECTRICAL AND ELECTRONICS ENGINEERING

Volume 17 Issue 4 Version 1.0 Year 2017

Type: Double Blind Peer Reviewed International Research Journal

Publisher: Global Journals Inc. (USA)

Online ISSN: 2249-4596 & Print ISSN: 0975-5861

Investigation of A Reciprocatory Driven Heat Loop to High Heat Single Phase Liquid Cooling for Temperature Uniformity

By O.T. Popoola & Y. Cao

Florida International University

Abstract- A bellows-type Reciprocating-Mechanism Driven Heat Loops (RMDHL) is a novel heat transfer device that could attain a high heat transfer rate through a reciprocating flow of the working fluid inside the heat transfer device. This paper investigates the possibility of applying the device for single phase liquid cooling for high performance computing. The objective of this paper is to apply the RMDHL to a liquid cooling system and compare its performance with a continuous cooling system. A Computational Fluid Dynamic (CFD) code that is validated experimentally was employed to numerically simulate both the Dynamic Pump Driven Heat Loop (DPDHL) and the reciprocating loop. To confirm the validity of the Numerical code to satisfactorily predict the reciprocating flow in the RMDHL, an experimental procedure was used to validate the Numerical Code.

Keywords: *heat loop, reciprocating flow, cooling, heat flux.*

GJRE-A Classification: *FOR Code: 290502, 290501*



Strictly as per the compliance and regulations of:



© 2017. O.T. Popoola & Y. Cao. This is a research/review paper, distributed under the terms of the Creative Commons Attribution-Noncommercial 3.0 Unported License <http://creativecommons.org/licenses/by-nc/3.0/>, permitting all non commercial use, distribution, and reproduction in any medium, provided the original work is properly cited.

Investigation of A Reciprocatory Driven Heat Loop to High Heat Single Phase Liquid Cooling for Temperature Uniformity

O.T. Popoola ^α & Y. Cao ^σ

Abstract- A bellows-type Reciprocating-Mechanism Driven Heat Loops (RMDHL) is a novel heat transfer device that could attain a high heat transfer rate through a reciprocating flow of the working fluid inside the heat transfer device. This paper investigates the possibility of applying the device for single phase liquid cooling for high performance computing. The objective of this paper is to apply the RMDHL to a liquid cooling system and compare its performance with a continuous cooling system. A Computational Fluid Dynamic (CFD) code that is validated experimentally was employed to numerically simulate both the Dynamic Pump Driven Heat

Loop (DPDHL) and the reciprocating loop. To confirm the validity of the Numerical code to satisfactorily predict the reciprocating flow in the RMDHL, an experimental procedure was used to validate the Numerical Code. This work proposes an efficiency term based on the temperature uniformity and overall performance, and compare both systems based on the proposed efficiency term. It was discovered that for temperature uniformity, the RMDHL performed better than the DPDHL with an efficiency of more than 30%.

Keywords: heat loop, reciprocating flow, cooling, heat flux.

Nomenclature

A	Area	[m ²]	<i>Subscript</i>	
C_p	Specific heat	[J/kg K]	<i>ave</i>	average value
D_i	Inside tube diameter	[m]	<i>c</i>	condenser
D_o	Tube outside diameter	[m]	<i>e</i>	evaporator
D_h	Hydraulic diameter	[m]	<i>in</i>	inlet
H	Height of rectangular channel	[m]	<i>m</i>	mean value
h	Heat-transfer coefficient	[W/m ² K]	<i>min</i>	minimum value
k	Thermal conductivity	[W/m ² K]	<i>max</i>	maximum value
L	length		<i>n</i>	direction normal to the wall
n	Reciprocating pump stroke frequency	cycles/s	<i>out</i>	outlet
\dot{m}	Mass flow rate	[kg/s]	<i>p</i>	pump piston
Nu	Nusselt number: $h/(k/D_h)$		<i>s</i>	surface
p	pressure	[Pa]	<i>t</i>	tubing
\dot{Q}	Heat-transfer rate	[W]	<i>w</i>	wall
q	volume flow rate	[m ³ /s]	<i>Superscript</i>	
Re	Reynolds number: $(\rho VD)/\mu$		= -	time-averaged quantity
Re_ω	kinetic Reynolds number: $\frac{\omega x_{max}^2}{\nu}$	[m]	→	vector
r	Tube inside radius	[m]		
S	Stroke	[m]		
T	Temperature	[°C]		
U	Overall heat-transfer coefficient	[W/m ² K]		
t	time	s		

Author ^α ^σ: Department of Mechanical and Materials Engineering, Florida International University, Miami, Florida, USA.
e-mail: opo002@fiu.edu

For the RMDHL, the requirement for the numerical for the inlet and outlet boundary conditions is a challenge, as it involves specifying the inlet and outlet in the same geometric position. Depending on the flow direction, inlet and outlet interchange. The outlet and the inlet in the forward direction become the inlet and outlet in the reverse direction. Additionally, the fluid conditions at the outlet and inlet of the model are interdependent for both the forward and reverse flow; the outlet flow conditions determine the value of the inlet flow conditions. The numerical studies reviewed failed to provide details on how to resolve the inlet and outlet boundary condition of the oscillating flow or simply modelled the loop driver using a fluid structure interaction (FSI) model. FSI modelling for the RMDHL requires costly computational resources because the number of mesh node in the driver is more than double the number of nodes in the rest of the RMDHL loop.

This study aims to empirically compare the performance of RMDHL to that of an existing liquid cooling systems, a dynamic pumps driven heat loop (DPDHL). This experimental and numerical study looks into the heat transfer and fluid flow aspects of the (RMDHL). Using a commercial CFD software and a novel numerical code, this study proposes an open loop configuration of the reciprocating flow. The proposed open loop configuration is developed based on the laminar model of T. S. Zhao and Cheng [20] and it seeks to reduce the computational cost of the numerical study by eliminating the need for fluid structure interaction study. It is expected that for future studies, the open loop configuration will reduce computational cost at the same time provided the accuracy required. To establish the accuracy of the Numerical codes, the results of the simulation were validated with appropriate experimental data. The study will also present the results of the validation of the CFD model and then compare the performance of a RMDHL with the DPDHL in terms of temperature, uniformity and heat removal from the surface of the heat source. For the current study a 3D, turbulent flow setup of continuous and RMDHL cooling loops with liquid water as the cooling fluid is provided. The setup and its results will be the foundation for the turbulent two phase model for various cooling fluids. It is expected that the completed model will be used to effectively evaluate the general concepts of RMDHL for future development and optimization of a standard industrial product.

II. CONCEPTUAL DESIGN OF THE BELLOW-TYPE RMDHL

The construction of the RMDHL and the specification of the design parameters remain as specified by [6]. For the schematic of the RMDHL represented in Fig. 1b, the most important relation that

describes the critical requirement for the operation of the heat loop is given as [6]:

$$ApS \geq AcLC + 2AtLt + AeLe \quad (1)$$

The length and average interior cross-sectional area of the evaporator are denoted by Le and Ae , respectively, the length and average interior cross-sectional area of the connection tubing between the evaporator and the condenser are Lt and At , the length and interior cross-sectional area of each condenser section are Lc and Ac . The piston cross-sectional area and reciprocating stroke are Ap and S , respectively. From the geometry of the heat loop Fig 1b and consideration of all the components of the RMDHL designed in equation (1), the critical S was calculated as 7 cm. A value of 7.62 cm was used for the reciprocating driver.

III. PERFORMANCE EVALUATION OF THE MODEL BELLOW-TYPE RMDHL

The experimental setup for the bellows-type RMDHL demonstration model is similar to the setup shown in Fig. 2a. The setup includes electric heaters for supplying heat to the cold plate of the heat loop, a DC power supply to the reciprocating driver, a control circuit board to control the reciprocating frequency of the driver, a constant temperature circulator to maintain a constant coolant inlet temperature of 10°C to the condenser, which would also control the operating temperature level of the heat loop, a data acquisition system, and the fabricated heat loop. Eight Omega flexible heaters (four on each side of the cold plate) are clamped by two aluminum plates onto the cold plate with insulation layers sandwiched between the heaters and clamping plates. Each heater has a dimension of 2 cm by 12 cm and could provide a heat input up to 200 W [6].

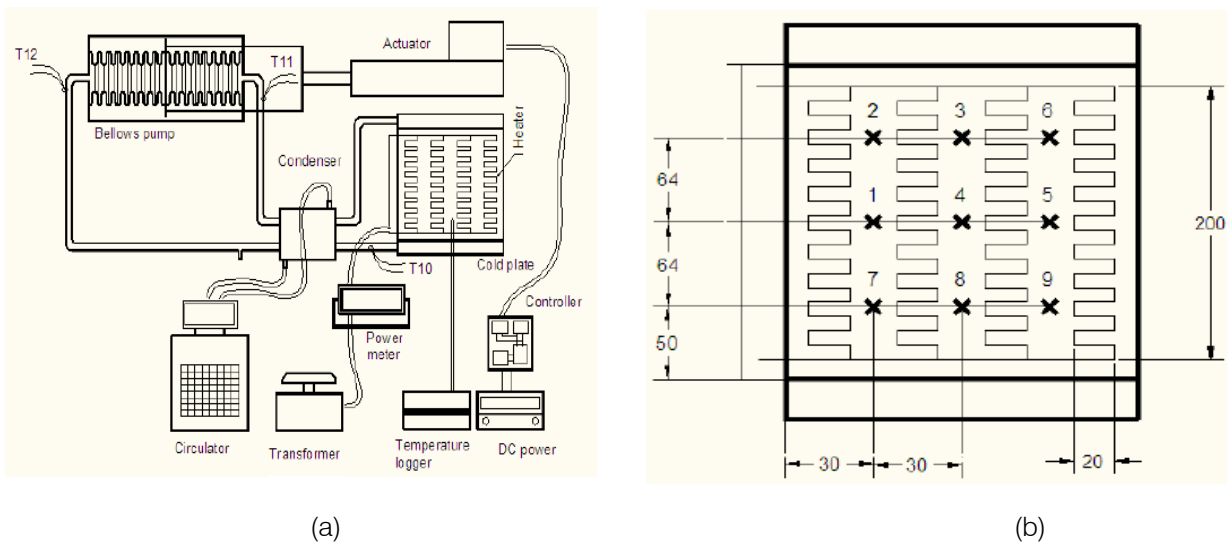


Fig. 2: Experimental setup: (a) Overall arrangement and (b) Thermocouple locations on the cold plate (size in mm).

Twelve thermocouples were placed at different locations of the heat loop. Nine of them (numbered as No. 1 through No. 9) are placed on the top surface of the cold plate at different locations for the study of temperature uniformity on the cold plate. Figure 2b shows detailed locations of these thermocouples. One thermocouple is placed near the condenser and another two thermocouples are placed on two ends of the bellows pump to monitor the heat loop temperature distribution in addition to those on the cold plate. These three thermocouples are numbered, respectively, as T10, T11, and T12, as shown in Fig. 2b.

During the experimentation, the heat loss from the clamping plate to the ambient was amounted to be less than 1%. Therefore, the sources of the experimental uncertainty were primarily due to the instruments themselves. The scanning thermocouple thermometer has an accuracy of $\pm 0.1\%$ of reading $\pm 0.4^\circ\text{C}$. The power meter has an accuracy of $\pm (1\% \text{ reading} + 5 \text{ digits})$. So the maximum uncertainty for the temperature and heat power measurements would be 1.0% and 2%, respectively.

IV. NUMERICAL ANALYSIS

It should be mentioned that the RMDHL can work either a single-phase cooling loop or two-phase cooling loop. In this study a single-phase application. A Computational Fluid Dynamic (CFD) code was employed to numerically simulate both the Dynamic Pump Driven Heat Loop (DPDHL) and the reciprocating loop. The first step of the model development was the generation of a 3D CAD model of the process by Solid Works. The condenser and evaporator loops are enclosed with solid wall. The two loops are separated from each other by the wall of the part body. The solid walls are aluminum and thermo physical properties for them are obtained from the fluent database. The

working liquid in the both loops is water. The heat fluxes are applied on both side of the evaporator and the boundary conditions are presented in the Table 1.

The schematic for the RMDHL is presented in Figure 3. The configuration for the geometry for the numerical model of the RMDH loop and the mesh grid distribution for numerical simulations of the RMDH loop is shown in Fig. 3c. The displacement of the piston $x_p(t)$ with time is [21]:

$$x_p(t) = -\frac{1}{2}S - \frac{1}{2}S \cos(\omega t) \quad (1)$$

$$u = u_{max} \sin(\omega t) \quad (2)$$

$$n = \omega / (2\pi) \quad (3)$$

The pressure gradient takes the form:

$$-\frac{1}{\rho} \frac{\partial p}{\partial x} = a e^{i\omega t} \quad (4)$$

Reynolds number for the reciprocating flow in the main pipe is given by:

$$Re_\omega = \frac{\omega D}{\nu} \quad (5)$$

Table 1: Dimensions, geometries and boundary conditions for the present cooling loop

Boundary conditions	Values and their ranges.	
Inlet velocity of the evaporator	varying stroke (cm)	7.62, 8.62, 9.62, 10.62
	frequency (n)	0.14, 0.28, 0.42, 1
Inlet velocity of the condenser	1.223 m/s	
Inlet temperature of the condenser	283 K	
Solid wall thickness	0.0001 m	
Heat (Q)	Heat (W)	Heat Flux (W/m ²)
	551	7983
	500	7244
	455	6592
	400	5795

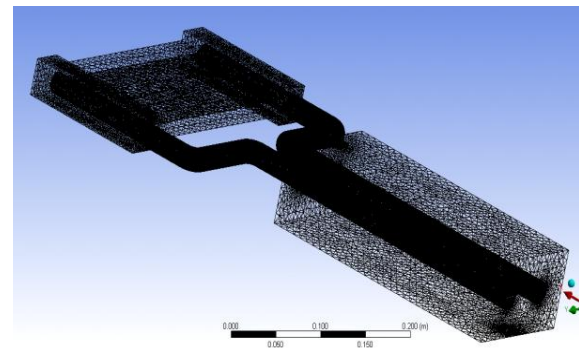
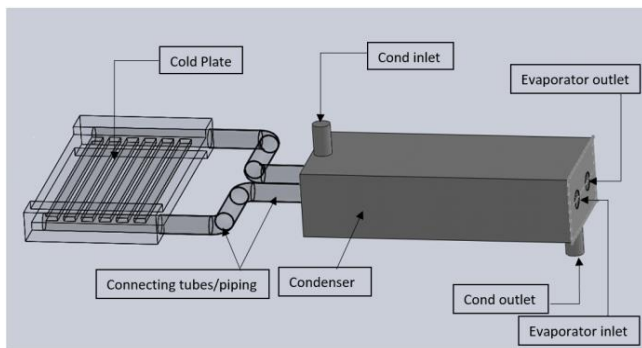
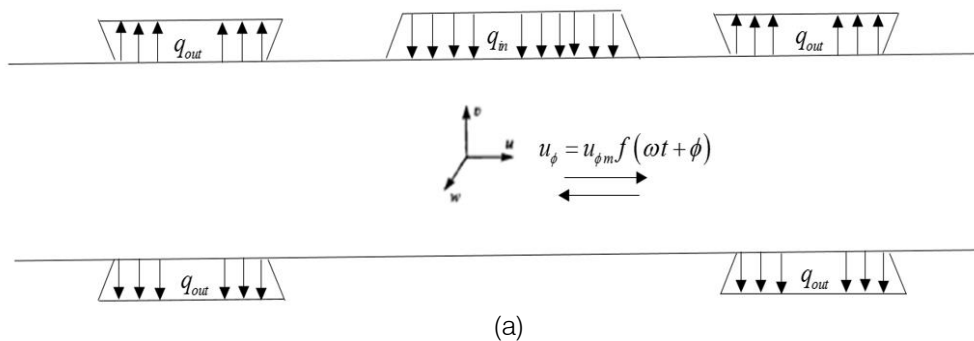


Fig. 3: (c) Geometry of the RMDH loop used for numerical model (b) Geometry of the RMDH loop used for numerical model (c) Grid distribution for the RMDH loop

Selection of the velocity for the DPHL was based on the average velocity was applied to the DPDHL system but increased by a factor of 22/14. In the present study for the DPDHL loop the following assumptions are made:

- (i) Both fluid flow and heat transfer are in steady-state and two dimensional.
- (ii) Fluid is in single phase and flow and turbulent.
- (iii) Properties of both fluid and heat sink materials are temperature independent.
- (iv) All the surfaces of heat sink exposed to the surroundings are assumed to be insulated except the walls of evaporator where constant heat flux

simulating the heat generation from different components.

V. GOVERNING EQUATIONS

As stated earlier, an open loop configuration of the heat loop is modeled. A C++ numerical code was used to determine the interfacial conditions between the end of the condenser and the pump. In this case, only a constant average temperature is initiated for the computation process and the final working fluid temperature at the interface had been determined through the iteration of the computational procedure. Even if physically the loop is open, the function has

actually closed the loop from the computational point of view. The open loop is used to reduce the computational cost of solving the whole domain and to avoid the simulation of the bellows part which requires an FSI modeling. The constant heat flux condition is applied at the outer surface of the cold plate while the rest of the exterior surface of the loop was insulated. A constant temperature is applied at the inlet of the condenser cooling water.

The geometry and thermal boundary conditions for the RMDHL is a bit more complex than the DPDHL. DPDHL will have permanent inflow and outflow regions, where one can easily define the inlet velocity and temperature boundary conditions. RMDHL flows require interchange between the inflow and out-flow boundaries during a cycle. For most applications, it is difficult to determine the inflow/outflow boundary conditions, since fluid particles exiting the flow domain during a part of the cycle are fed back into the domain, later in the cycle. The DPDHL which represents the case of forced convection heat transfer in channels and tubes is well understood. Based on above assumptions, the governing equations for fluid and energy transport are:

Fluid flow:

$$\nabla \cdot V = 0 \quad (6)$$

$$\rho(V \cdot \nabla V) = -\nabla p + \mu \nabla^2 V \quad (7)$$

Energy in fluid flow

$$\rho c_p (V \cdot \nabla T) = k \nabla^2 T \quad (8)$$

Energy in heat sink solid part

$$k_s (\nabla^2 T_s) = 0 \quad (9)$$

The boundary conditions for these equations are specified in the previous table. Based on the operating conditions described above, the boundary conditions for the governing equations are given as:

Inlet:

$$V = V_{in}, \quad T_{in} = (T_{out})_{ave} \quad (10)$$

Outlet:

$$P = P_{out}, \quad \frac{\partial T}{\partial n} = 0 \quad (11)$$

Fluid–solid interface:

$$V = 0, \quad T = T_s, \quad -k_s \frac{\partial T_s}{\partial n} = -k \frac{\partial T}{\partial n} \quad (12)$$

At the top wall:

$$q_w = -k_s \frac{\partial T_s}{\partial n} \quad (13)$$

In Eq. (9), V_{in} and T_{in} are the fluid inlet pressure and temperature, respectively; P_{out} is the pressure at the

outlet, n is the direction normal to the wall or the outlet plane, and q_w is the heat flux applied at the top wall of the heat sink.

VI. RESULTS AND DISCUSSION

Details of the numerical solution scheme are presented in Table 2. The CFD numerical algorithm utilizes Pressure Implicit with Splitting of Operators (PISO) formulation for the solution of the Navier-Stokes and heat transport equations. Gradient discretization was Green-Gauss Node based, pressure discretization was Second order while the momentum and energy discretization were Second order upwind. Transient formulation was second order Implicit. Appropriate under relaxations were used to improve the numerical stability for all governing equations. The solver conditions for the DPDHL are similar to those for conventional unidirectional flow. The criteria for convergence was set at 10^{-4} for the continuity and x, y and z momentum. While a convergence criterion of 10^{-8} was set for the DPDHL and 10^{-6} for the RMDHL.

The resulting computational mesh is presented in Fig. 3c. In order to establish computational accuracy, grid independence studies are always necessary and were equally performed in this work. The mesh independence studies were conducted for two more grids with coarse and fine meshes settings. The variation of the results between the coarsest and finest meshes was 5% (the largest variation). However, for the mesh used for the numerical simulation the results showed less than 1.5% variation for the last two grid size.

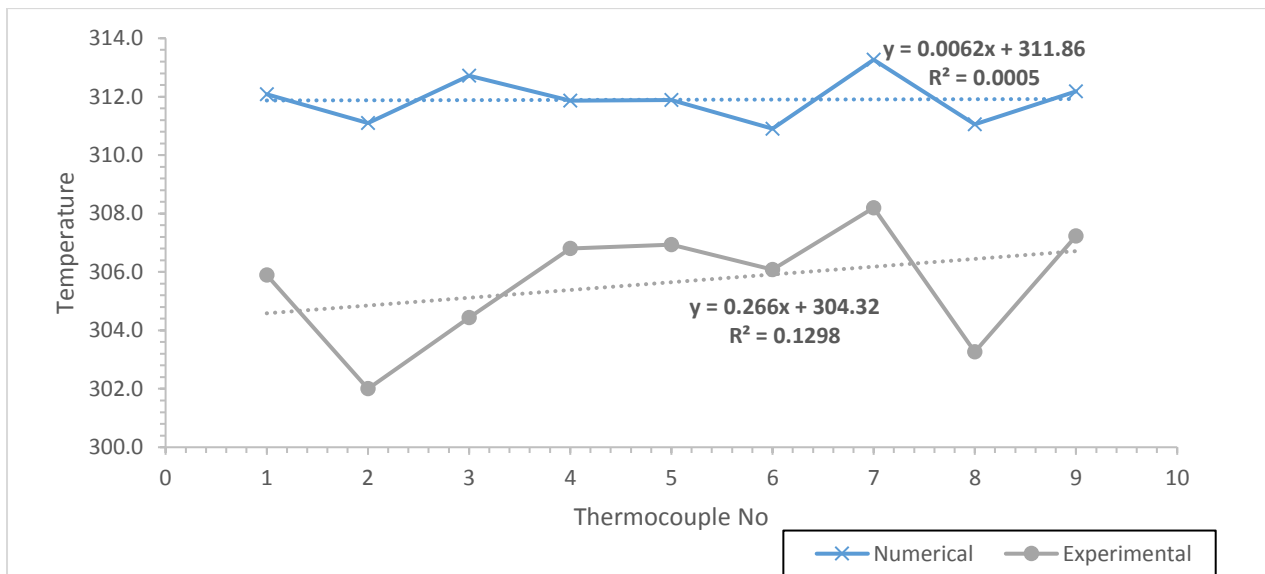
Fig 4 show the comparism of the results for the experimental data and the Numerical results for the RMDHL loop. This comparism shows that the values of the numerical model are significantly higher than those of the experimental data. However, statistical comparism using the best-fit regression, the Nash-Sutcliffe efficiency (NSE), the percentage bias (PBIAS) and RMSE-observations standard deviation ratio (RSR) table 3 show that the results of the computational study were compared with the experimental work and in general, good agreement with experimental data within acceptable limits. Details in Fig 4 and Table 4. As is widely adopted, NSE determines the relative magnitude of the residual variance ("noise") compared to the measured data variance ("information"). NSE ranges between $-\infty$ and 1.0, the closer NSE is to 1, the more accurate the prediction. PBIAS measures the average tendency of the simulated data to be larger or smaller than the experimental data, the lower the magnitude the more accurate the model simulation, and the optimal value would therefore be zero. RSR measures the error index and like the PBIAS, its optimal value is zero. Hence the numerical solution was used as the basis for the comparism.

For the RMDHL, the temperature profile is more uniform than the temperature profile for the DPDHL. Table 4 and Table 5 show that not only is the mean temperature for the RMDHL lower than the mean temperature for the DPDHL, the standard deviation around the mean is about 1.5°C for the RMDHL and about 5°C for the DPDHL. It will be observed that there is an average of about 7% difference when the average value of the numerical model is compared to the data collected. This is because the actual numerical modeling of the reciprocating flow would require a Fluid structure interaction (FSI) of the pump. To reduce computational costs associated with the FSI, This study adopted a 'virtual loop' analysis, a numerical code in C. The virtual loop assumed complete perfect mixing of the fluid in the pump and assigns the mean parameter formulation to inlets and outlets as flow direction changes. The details of the Virtual loop has been presented in details in [22]. The maximum temperature occurs at the midpoint of the walls while the maximum temperature for the DPDHL is at the exit side of the cold

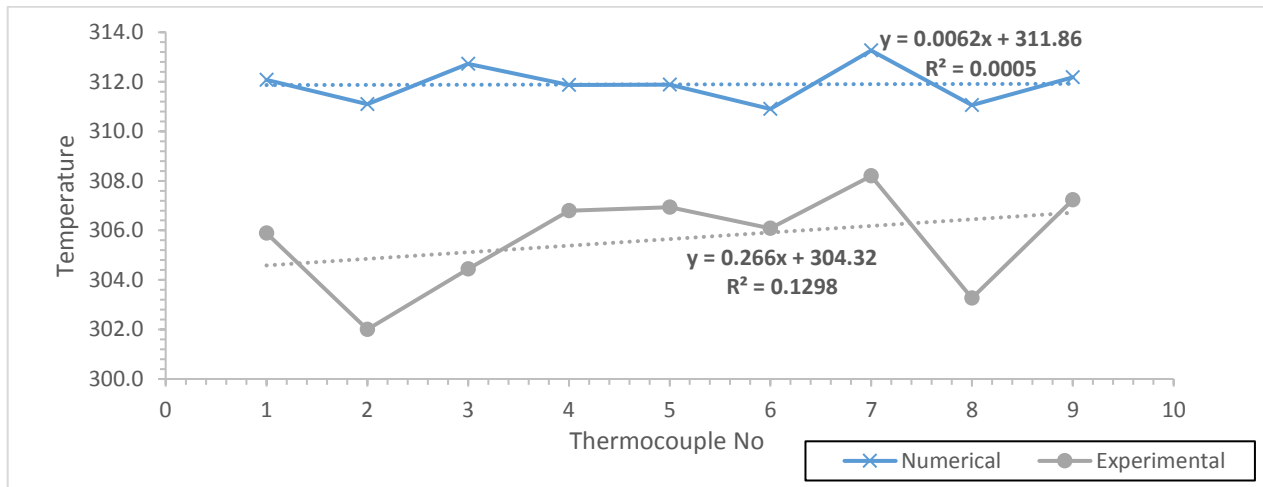
plate. In terms of performance; thus, the RHMDL is more effective in cooling the plate than the DPDHL by up to 5°C. As shown in Table 5, for a heat transfer rate of 550 W, 500 W, 450 W, 400 W, the DPDHL produced an average hot plate temperature of 331.71, 327.77, 323.18, and 318.19°C, respectively; while the RMDHL produced an average of 328.09, 327.31, 324.37 and 313.19°C, respectively. The basis for determining the average hot plate temperature is provided in Equation (16). The reason for the better performance is that RMHDL is that rate of heat loss to the condenser is higher for the RMDHL than for the DPDHL. Fig 5 and Fig 6 shows the temperature distribution across the evaporator plate for RHMDL at 550 W and 450 W and also the DPDHL for 550 W and 450 W. The colder sections represent the portion of the evaporator in contact with the condenser. The reciprocating loop maintains a higher on the condenser side than the continuous loop and this represents a higher heat removal rate from evaporator by the reciprocatory loop.

Table 2: Details of the Numerical solution variables

Solver parameters	Solver parameters Values
Solution Method	PISO
Time step (s)	0.5
Relaxation factor momentum	0.4
Relaxation factor pressure	0.3
Relaxation factor energy	0.9



(a)



(b)

Fig. 4: Comparison of numerical and experimental Temperature distributions over the cold plate at different heat inputs for a coolant inlet temperature of 10°C (a) 550 W (b) 400 W

Table 3: Results for statistical comparism of experimental and Statistical results

Thermocouple No	Temperature (K)	550W		400W	
		Experimental	Numerical		
1		305.9	312.1	301.8	307.8
2		302.0	311.1	297.7	307.0
3		304.4	312.7	299.9	308.0
4		306.8	311.9	302.0	307.0
5		306.9	311.9	303.0	308.2
6		306.1	310.9	302.1	306.9
7		308.2	313.3	302.9	308.2
8		303.3	311.1	299.0	307.1
9		307.2	312.2	303.1	308.1
Regression	R2	0.1	0.0	0.1	0.0
	Slope	0.3	311.86	0.3	311.9
	Intercept (K)	304.32	311.86	304.3	311.9
NSE			-7.87		-7.9
PBIAS			-2.04		-2.1
RSR			2.98		3.0

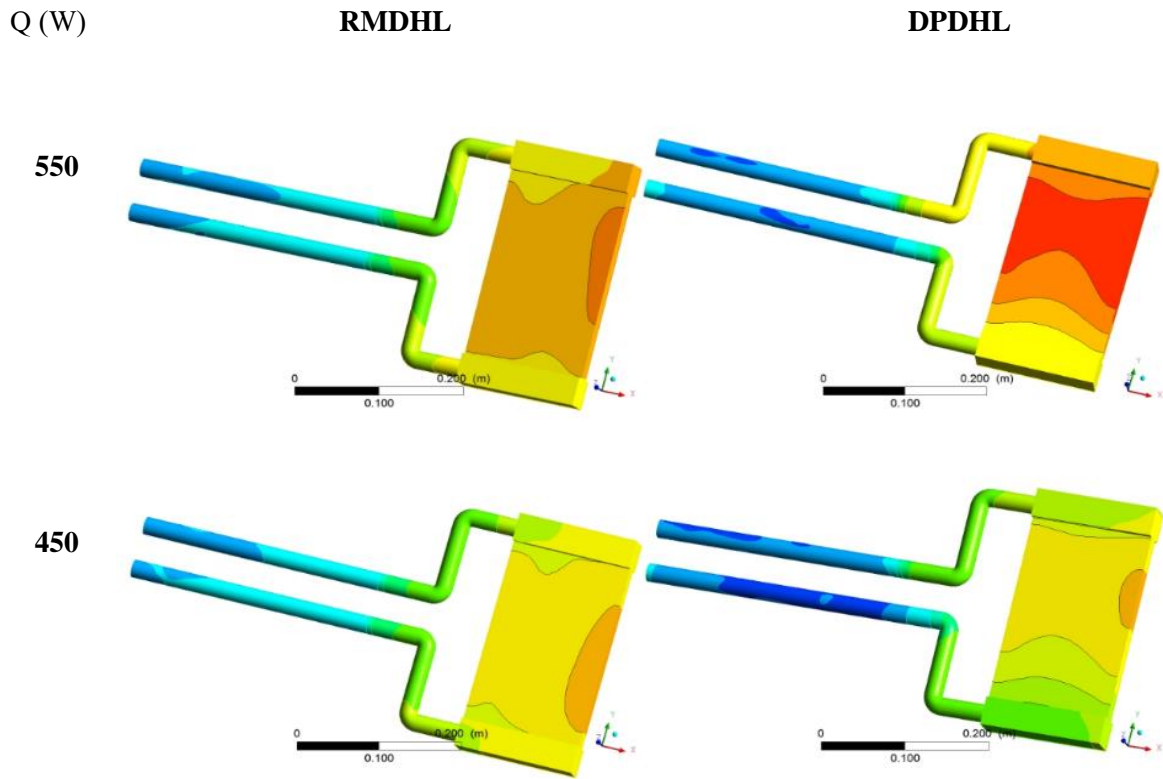
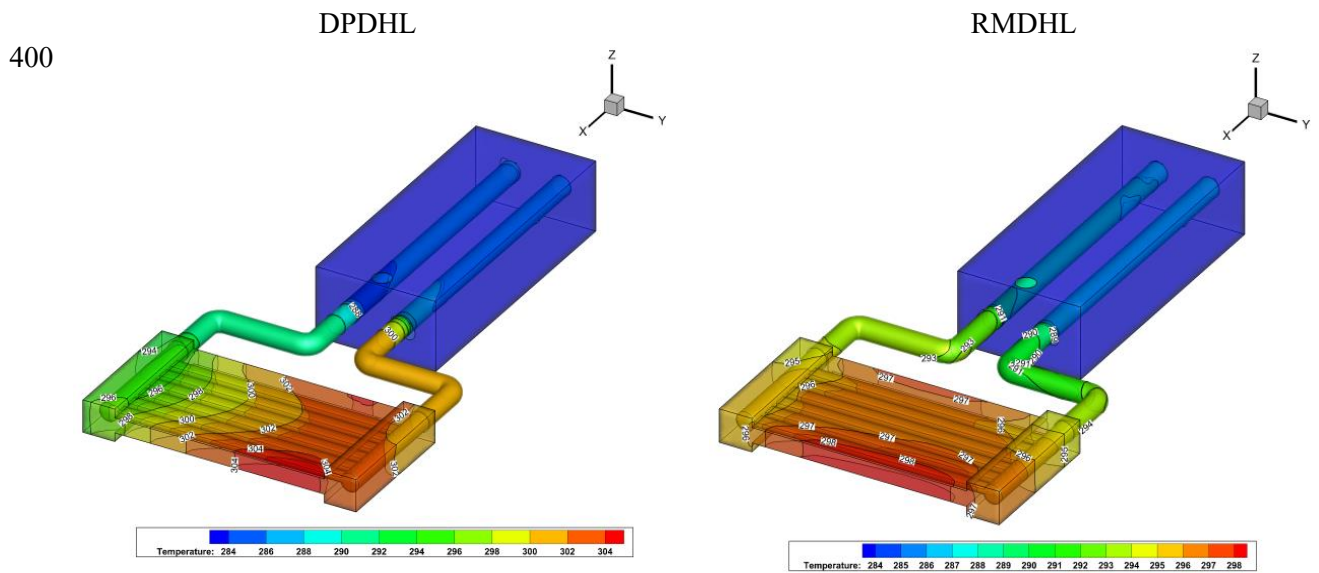
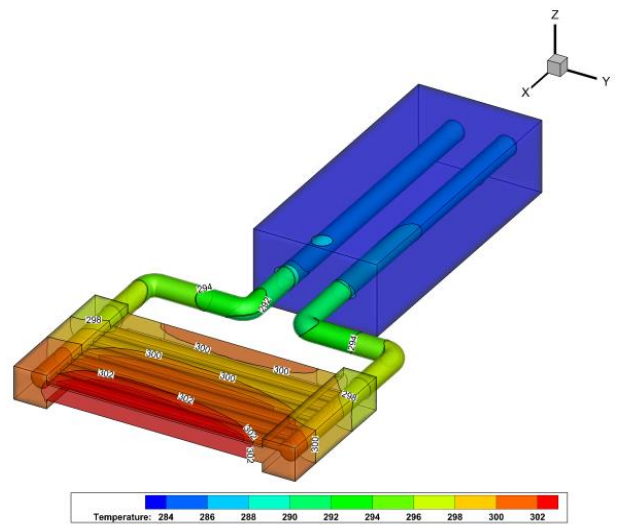
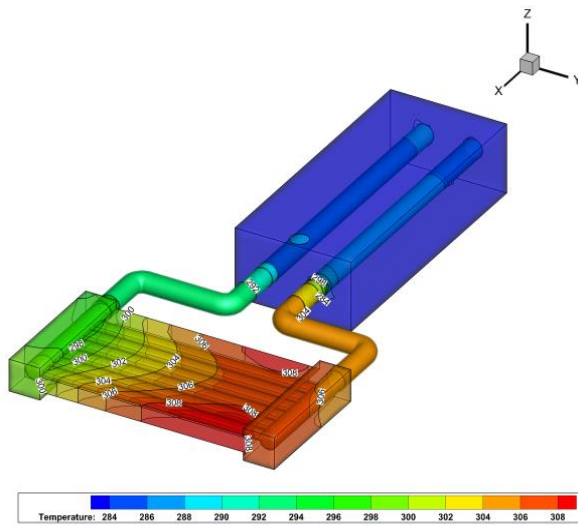


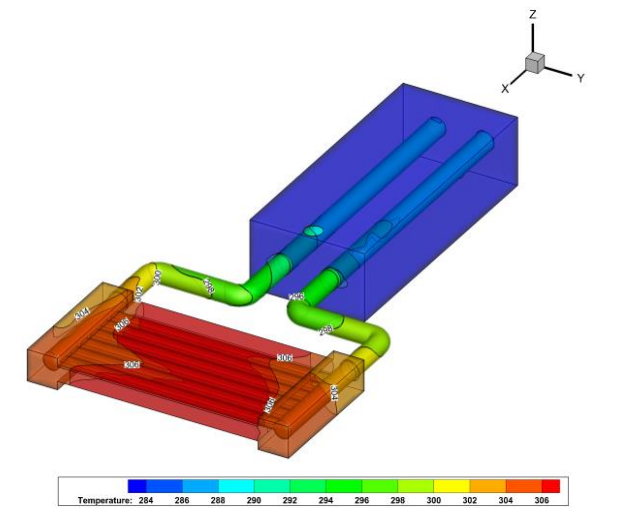
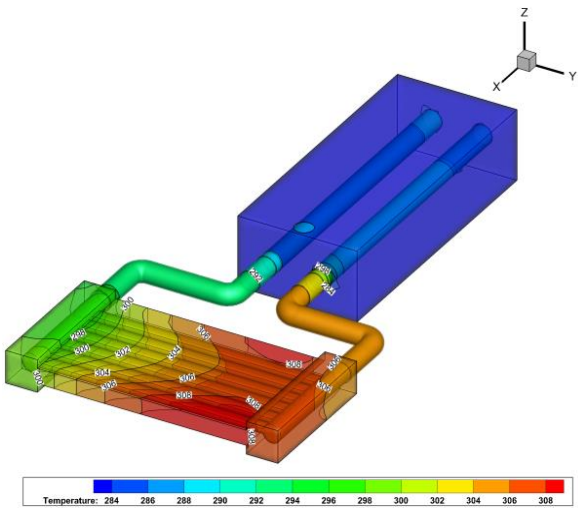
Fig. 5: Contour of varying temperature across evaporator for varying heat transfer rate



450



500



550

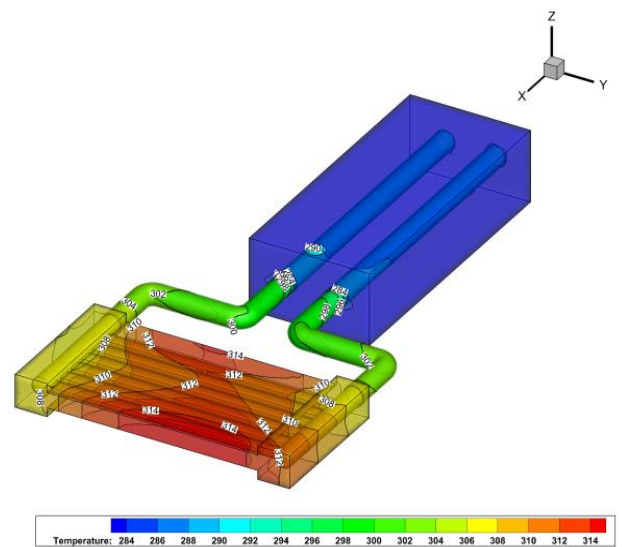
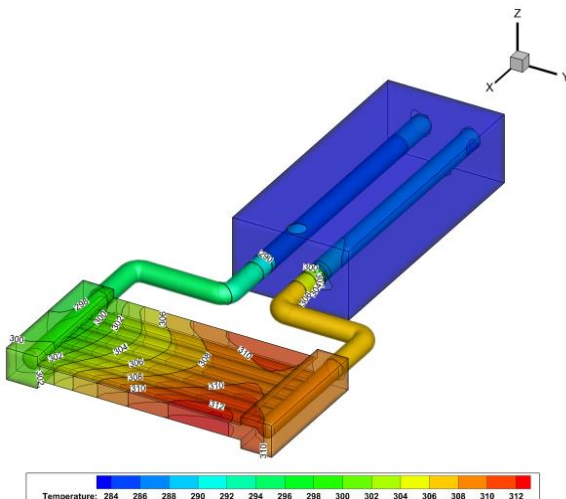


Fig. 6: Temperature contours of hot plate for various heat transfer rate and cooling methods

Another emphasis of this paper is the temperature uniformity over the cold plate. Fig 5 show the temperature continues loop for cold plate at a condenser inlet velocity of 1.23 m/s, heat transfer rate varying from 400W to 550W and inlet temperature of the condenser 283 K. The figures clearly show that the uniformity of the temperature profiles of the RMDHL is much higher than the uniformity of the DPDHL loop. As seen in Fig 6, there are two temperature gradients. One gradient along the evaporator and another gradient across the evaporator. The gradient along the evaporator is common to both the DPDHL and the RMDHL and is as a result of pressure drop along the piping in the evaporator. The effect of this gradient will vary if a different piping configuration is adopted.

The empirical variation of the temperature is investigated at 3 cross-sections. The cross sections are shown in Fig. 7, section A-A at one end, Section B-B at the center, and section C-C at the other end. Temperatures at the centerline was compared for both reciprocating and DPDHL flow at two heat transfer rate, 400 and 550 Wand compared statistically. Figure 8 and table 4 presents the details of the analysis. The plate temperature is minimum at the inlet of the evaporator and gradually increases toward the outlet of the outlet for the DPDHL flow loop. Another statistic indicator that may be used to gage the temperature uniformity over the cold plate is the standard deviation, defined [6] as:

$$\sigma_T = \sqrt{\frac{1}{N-1} \sum_{i=1}^N (T_i - T_m)^2} \tag{14}$$

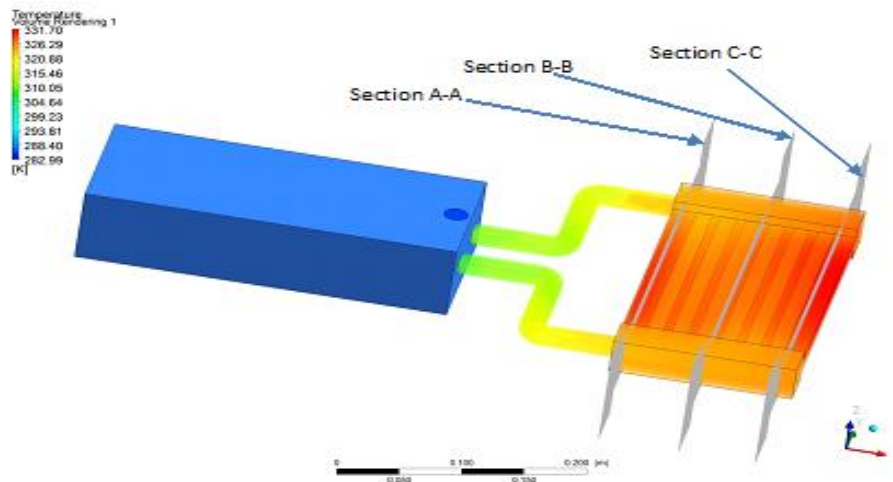


Fig. 7: Volume rendering of cross section of hot plate showing cross section for temperature

Table 4: Temperature variation across various cross sectional areas of the hot plate

Q(W)	DPDHL						RMDHL					
	400			550			400 RMDHL			550 RMDHL		
x (m)	T _{min}	T _{max}	ΔT	T _{min}	T _{max}	ΔT	T _{min}	T _{max}	ΔT	T _{min}	T _{max}	ΔT
0.01	305.90	321.80	15.93	314.70	336.80	22.05	304.90	313.50	8.58	317.10	330.00	12.84
0.03	305.90	321.20	15.33	314.80	336.00	21.22	306.10	313.00	6.88	320.30	329.20	8.97
0.04	306.00	320.60	14.64	314.90	335.10	20.24	307.10	312.80	5.70	321.40	328.50	7.11
0.06	306.00	320.40	14.36	314.90	334.70	19.83	307.50	313.40	5.85	322.80	328.50	5.71
0.08	306.10	320.70	14.53	315.10	335.10	20.01	308.40	314.20	5.79	323.10	328.80	5.71
0.10	306.70	321.10	14.39	315.50	335.60	20.05	309.60	315.10	5.51	323.30	329.60	6.25
0.12	306.80	322.00	15.15	316.10	336.80	20.73	310.20	316.20	6.01	323.80	331.00	7.16
0.14	311.90	322.40	10.58	323.10	337.40	14.38	312.20	316.70	4.57	325.60	331.60	5.98

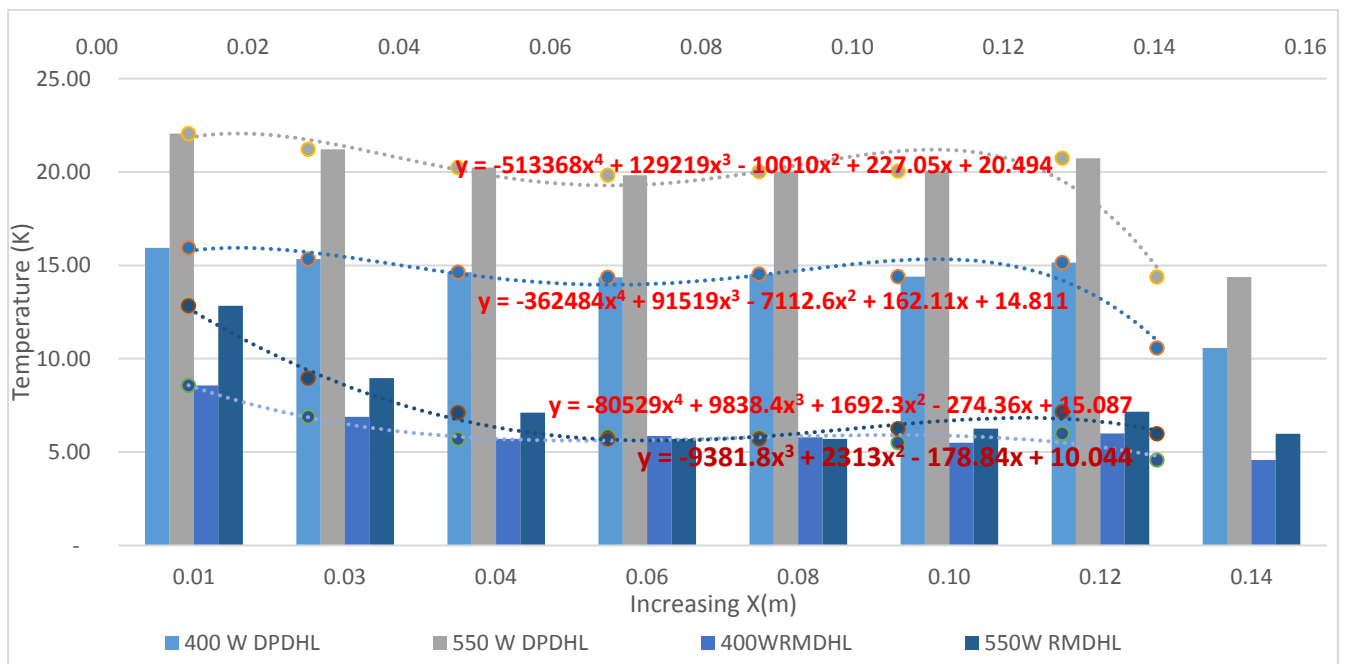


Fig. 8: Temperature variation across various cross sectional areas of the hot plate

Table 5: Standard deviation of temperature across cross sections of hot plate

	400W	550W	400W RMDHL	550W RMDHL
Section A-A	2.96	4.09	1.67	1.38
Section B-B	2.86	3.96	0.86	0.86
Section B-B	3.49	4.74	1.99	1.51

For this purpose, the steady-state minimum temperature, maximum temperature, and the temperature difference, at different power input for water coolant inlet temperatures of 10°C is shown in Table 1. Although the maximum temperature differences may vary with the power input, they are generally around 6°C for the RMDHL and 20°C for the DPDHL loop. The standard deviation for the RMDHL is less than half of the value for the DPDHL (Table 5).

The standards deviation of the RMDHL changes only slightly with increasing rate of heat transfer but for the DPDHL it increases significantly with increasing rate of heat transfer. It should be pointed out that all of the data presented herein are based on a low driver reciprocating frequency of 0.14/s for a maximum stroke. The figures show that not only is the mean temperature for the RMDHL lower than the mean temperature for the DPDHL, the standard deviation around the mean is about 1.5°C for the RMDHL and about 4°C for the DPDHL.

It should be pointed out that all of the data presented herein are based on a low driver reciprocating frequency of 0.14/s for a maximum stroke. The figures show that not only is the mean temperature for the RMDHL lower than the average temperature for the

DPDHL cooling loop, the standard deviation around the mean is about 1.5°C for the RMDHL and about 4°C for the DPDHL Fig. 9 reveals that although the variation in hot plat temperature is different for the RMDHL and the DPDHL, the variation in the range of the temperature is the same. The range is highest at the entrance; it begins to drop towards as the cooling proceeds towards the entrance. The range is flattening towards the middle with a slight inflection and continues to fall at the outlet of the fluid.

In a bid to determine the efficiency of both systems, this work also proposed a an expression for the Coefficient of Performance (COP) based on temperature. The requirement of adequate coefficient in predicting the system is that the coefficient must satisfies the second law of thermodynamics (Moran and Shapiro, 2004) and should be dependent on operating conditions, especially average plate temperature and relative temperature between sink and system. The coefficient is proposed in Equations 15 -17. The COP terms is similar to the term used for determination of the COP for carnot vapor refrigeration cycle. For the basis for selcting the cold reservoir and the hot reservoir is defined in Eq 18. The summary of the calculations is presented in Table 6. Table 6 shows the value of the

COP and the resulting efficiency is similar irrespective of the changing heat flux, and the various temperature parameters (Fig 9) used in computing the terms on the hot plate. The trend follows variations in similar terms in the literature (Moran and Shapiro 2004; Mcquiston et al. 2006). Ultimately the efficiencies show that the value of the efficiency of the RMDHL is about 30% higher than those attained by the DPDHL flow system (Fig 9b).

$$\eta_T = \frac{COP_{hpT}}{COP_{cpT}} \quad (17)$$

Thp = average temperature of hot plate (ATHP); Tcp = average temperature of cold plate (ATCP)

Thf = average temperature of hot fluid (ATHF); η_T = efficiency

$$COP_{cpT} = \frac{cp}{T_{hf}-T_{cp}} \quad (15)$$

$$T_i = \frac{\sum_{i=1}^n T_i}{n} \quad (18)$$

$$COP_{hpT} = \frac{T_{hf}}{T_{hp}-T_{hf}} \quad (16)$$

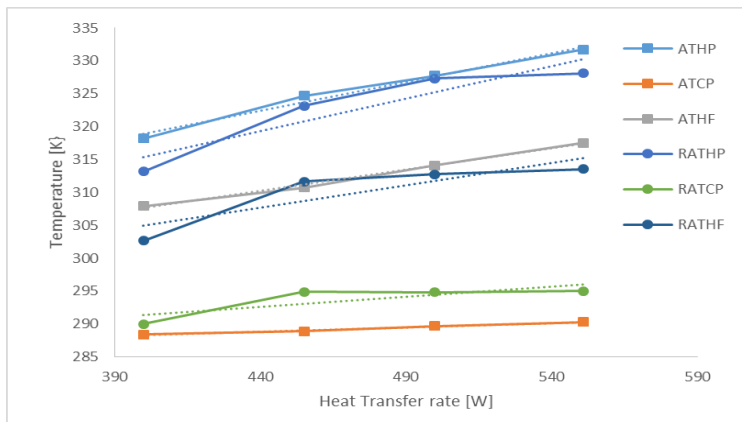
Table 6: Average temperature, standard deviation and efficiency of cooling systems

Cooling system	Parameter	Heat transfer rate Q[W]			
		551.00	500.00	455.00	400.00
DPDHL	ATHP (K)	331.71	327.77	323.18	318.19
	ATCP (K)	290.29	289.67	288.88	288.41
	COP _{hpT}	22.40	23.01	24.97	30.01
	ATHF (K)	317.54	314.12	310.74	307.93
	COP _{cpT}	10.65	11.85	13.21	14.77
	η	0.49	0.51	0.53	0.49
	σ_T (K)	3.88	3.54	3.17	2.83
RMDHL	ATHP (K)	328.09	327.31	324.37	313.19
	ATCP (K)	295.03	294.84	294.91	289.99
	COP _{hpT}	21.53	21.51	24.49	30.04
	ATHF (K)	313.53	312.76	311.64	303.10
	COP _{cpT}	15.95	16.45	17.62	22.12
	η	0.74	0.76	0.72	0.74
	σ_T (K)	1.51	1.34	1.51	1.62

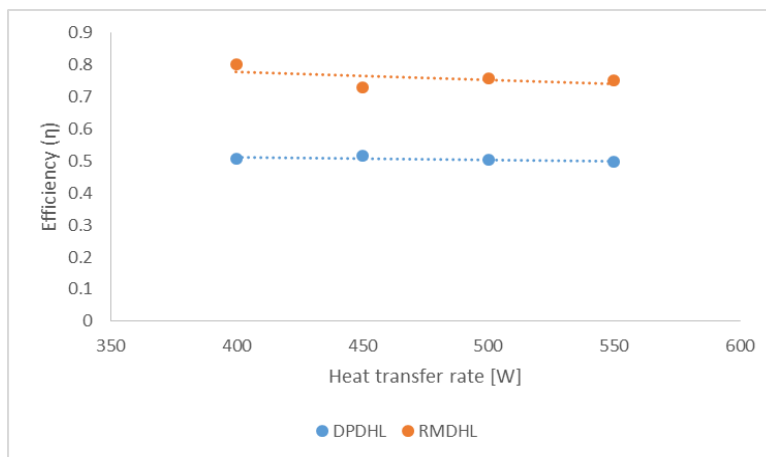
VII. CONCLUSION

A numerical model for the simulation of the RMDHL has been successfully built and validated by experimental data. The results indicate that the cooling efficiency of the RMDHL is meaningfully higher than that of the DPDHL with a reduced maximum temperature under the same heat input and cooling conditions. The results show that that the temperature increases with increase of heat flux on the walls or decrease of the flow rate. It was also shown that the temperature profiles are more uniform for an RMDHL loop compared to a DPDHL loop both in terms of temperature uniformity and efficiency.

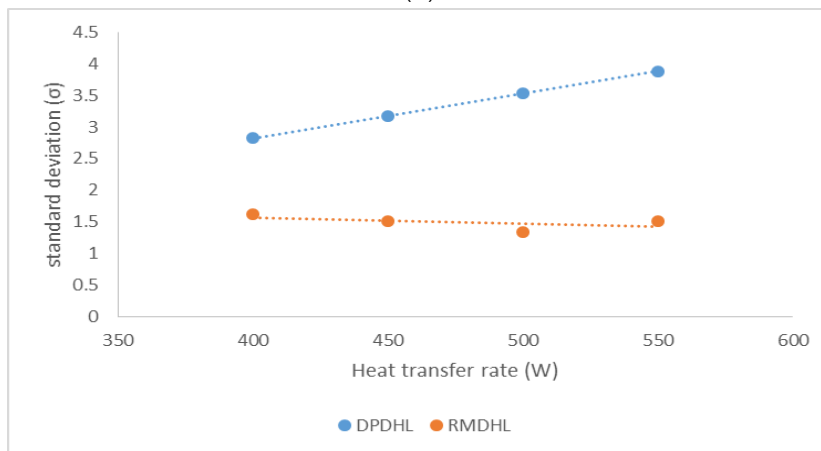




(a)



(b)



(c)

Fig. 9: Plot of Heat transfer rate and (a) average temperature (b) efficiency of cooling systems (c) standard deviation

REFERENCES RÉFÉRENCES REFERENCIAS

1. Z. Liu, S. Tan, H. Wang, Y. Hua, and A. Gupta, "Compact thermal modeling for packaged microprocessor design with practical power maps," *Integr. VLSI J.*, vol. 47, no. 1, pp. 71–85, Jan. 2014.
2. G. Hetsroni, A. Mosyak, and Z. Segal, "Nonuniform temperature distribution in electronic devices cooled by flow in parallel microchannels," *IEEE Trans. Components Packag. Technol.*, vol. 24, no. 1, pp. 16–23, 2001.

3. DARPA - Microsystems Technology Office, "Near Junction Thermal Transport (NJTT) DARPA-BAA-11-09," 2010.
4. Y. Cao and M. Gao, "Reciprocating-Mechanism Driven Heat Loops and Their Applications," in *ASME 2003 Heat Transfer Summer Conference Heat Transfer: Volume 1*, 2003, pp. 781–789.
5. Y. Cao and M. Gao, "Experimental and Analytical Studies of Reciprocating-Mechanism Driven Heat Loops (RMDHLs)," *J. Heat Transfer*, pp. 72901-1–6, 2008.
6. Y. Cao, D. Xu, and M. Gao, "Experimental study of a bellows-type reciprocating-mechanism driven heat loop," *Int. J. Energy Res.*, vol. 37, no. 6, pp. 665–672, May 2013.
7. Z. a. Williams and J. a. Roux, "Thermal Management of a High Packing Density Array of Power Amplifiers Using Liquid Cooling," *J. Electron. Packag.*, vol. 129, no. December 2007, p. 488, 2007.
8. T. L. Bergman, A. S. Lavine, and F. P. Incropera, *Fundamentals of Heat and Mass Transfer*, 7th ed. Hoboken, NJ: John Wiley, 2012.
9. M. Özdiñç Çarpınliođlu and M. Yařar Gündođdu, "A critical review on pulsatile pipe flow studies directing towards future research topics," *Flow Meas. Instrum.*, vol. 12, no. 3, pp. 163–174, Jun. 2001.
10. M. Gundogdu and M. Carpinlioglu, "Present State of Art on Pulsatile Flow Theory : Part 1: Laminar and Transitional Flow Regimes," *JSME Int. J. Ser. B Fluids Therm. Eng.*, vol. 42, no. 3, pp. 384–397, 1999.
11. M. Y. Gündođdu and M. Ö. Çarpınliođlu, "Present state of art on pulsatile flow theory, part 2. Turbulent flow regime," *JSME Int. J. Ser. B Fluids Therm. Eng.*, vol. 42, no. 3, pp. 398–410, 1999.
12. M. Ibrahim and W. Hashim, "Oscillating Flow in Channels with a Sudden Change in Cross Section," *Comput. Fluids*, vol. 23, no. 1, pp. 211–224, 1994.
13. Y. Su, J. H. Davidson, and F. A. Kulacki, "Numerical investigation of fluid flow and heat transfer of oscillating pipe flows," *Int. J. Therm. Sci.*, vol. 54, pp. 199–208, Apr. 2012.
14. M. Ghafarian, D. Mohebbi-Kalhari, and J. Sadegi, "Analysis of heat transfer in oscillating flow through a channel filled with metal foam using computational fluid dynamics," *Int. J. Therm. Sci.*, vol. 66, pp. 42–50, Apr. 2013.
15. L. Wang and X.-Y. Lu, "An investigation of turbulent oscillatory heat transfer in channel flows by large eddy simulation," *Int. J. Heat Mass Transf.*, vol. 47, no. 10–11, pp. 2161–2172, May 2004.
16. M. B. Ibrahim, Z. Zhang, and S. Kembhavi, "A 2-D axisymmetric CFD model of oscillatory flow with separation," in *Energy Conversion Engineering Conference, 2002. IECEC '02. 2002 37th Intersociety*, 2002, vol. 37, pp. 511–517.
17. M. M. Molla, M. C. Paul, and G. Roditi, "LES of additive and non-additive pulsatile flows in a model arterial stenosis.," *Comput. Methods Biomech. Biomed. Engin.*, vol. 13, no. July 2014, pp. 105–120, 2010.
18. C. Hsu, X. Lu, and M. Kwan, "LES and RANS Studies of Oscillating Flows over Flat Plate," *J. Eng. Mech.*, vol. 126, no. 2, pp. 186–193, Feb. 2000.
19. M. Zhao, L. Cheng, and H. An, "Three-dimensional numerical simulation of flow around a circular cylinder under combined steady and oscillatory flow," *J. Hydrodyn. Ser. B*, vol. 22, no. 5, pp. 144–149, Oct. 2010.
20. T. S. Zhao and P. Cheng, "A Numerical Study of Laminar Reciprocating Flow in a Pipe of Finite Length," *Appl. Sci. Res.*, vol. 59, pp. 11–25, 1998.
21. J. De-Jongh and R. Rijs, Eds., *Pump Design*. Veldhoven: Arrakis, 2004.
22. O. T. Popoola, A. Bamgbade, and Y. Cao, "Numerical Modelling of Reciprocating flow Using a Virtual Loop," in *2nd Thermal and Fluids Engineering Conference (TFEC)*, 2017, p. Unpublished.
23. M. J. Moran and H. N. Shapiro, *Fundamentals of Engineering Thermodynamics*. 2004.
24. F. C. Mcquiston, J. D. Parker, and J. Spitler, *Heating, ventilating, and air conditioning: Analysis and design*. 2006.

This page is intentionally left blank